photonics

MDPI

Communication

Grating Pair Wavepacket Shaper for Crafting Spatiotemporal Optical Vortices with Arbitrary Tilt Angles

Jordan Adams [1] and Andy Chong [2,3,*]

[1] RF and Optics, Riverside Research Institute, Beavercreek, OH 45431, USA; adamsj22@udayton.edu
[2] Department of Physics, Pusan National University, Busan 46241, Republic of Korea
[3] Institute for Future Earth, Pusan National University, Busan 46241, Republic of Korea
* Correspondence: chong0422@pusan.ac.kr

Abstract: Spatiotemporal optical vortices with arbitrary tilt angles can be generated by adjusting spatial chirp and beam size at a phase modulation plane in a pulse shaper setup. A grating pair setup is proposed to generate variable spatial chirp independent of the beam profile. The initial dispersion of the pulse allows for the independent control of the vortex orientation. By adjusting the beam size, spatial chirp, and initial dispersion, arbitrary vortex orientation across all the possible angles can be achieved. The ability to achieve arbitrary vortex orientations at long propagation distances could offer significant advantages for long-distance communication applications.

Keywords: orbital angular momentum; optical vortex; spatiotemporal optical vortex

Received: 30 November 2024
Revised: 16 January 2025
Accepted: 27 January 2025
Published: 31 January 2025

Citation: Adams, J.; Chong, A. Grating Pair Wavepacket Shaper for Crafting Spatiotemporal Optical Vortices with Arbitrary Tilt Angles. *Photonics* **2025**, *12*, 126. https://doi.org/10.3390/photonics12020126

1. Introduction

Optical vortices have been extensively researched for decades [1] and have given rise to applications from particle manipulation [2] to microscopy [3]. One of the most common applications for optical vortices has been long-distance free-space communication [4] where these vortices allow data transfer at higher bandwidths.

In contrast, spatiotemporal vortices are a new type of optical vortex, with the OAM being transverse to the propagation direction [5,6]. Recently, vortices with an arbitrary spatiotemporal tilt angle have been theoretically investigated and demonstrated experimentally by a variety of methods [7–11]. In these cases, the vortex orientation lies at an angle between transverse and parallel directions to propagation. Tilted vortices may offer advantages, particularly in free-space communication, where the tilt angle could serve as an additional degree of freedom and enhance bandwidth. However, the experimentally demonstrated tilted vortices were localized near the focus of a beam [7,8]. Additionally, it has been recently shown that the tilt angle changes with propagation [11]. Consequently, a full characterization of the tilt angle change with propagation is needed to enable the application in free-space communication.

This work broadens the application of tilted vortices to long-distance scenarios, providing a theoretical investigation to set the desired tilt angle of the vortex at a specific distance. In contrast to a typical pulse shaper setup, we propose a grating pair to control the spatial chirp of the wavepacket. In such a wavepacket shaper, a spatial light modulator (SLM) is used to control the wavepacket. Having a large beam size along with variable spatial chirp at the spatial light modulator plane enables the encoding of a user-defined tilted vortex phase in space and time. By such a wavepacket shaper, we show that the grating pair separation can control the vortex angle. Additional vortex orientation angle adjustments can be obtained by varying the initial dispersion. Finally, adding a telescope system can

enable a reasonable beam size at the desired location. Controlling several parameters in the optical system allows for generating spatiotemporal vortices at any desired angle.

2. Results

The concept is shown in Figure 1. A pulsed beam emerges on a grating pair of variable separations, causing frequencies to be dispersed spatially, resulting in a spatially chirped beam on the SLM plane. Since there is no lens to focus, the beams of each frequency strongly overlap spatially, as shown in Figure 1. It is also important to note that larger beams will have more overlap. As a spiral phase is applied to the SLM, a tilted vortex phase is acquired in addition to the temporal dispersion accumulated by the grating pair.

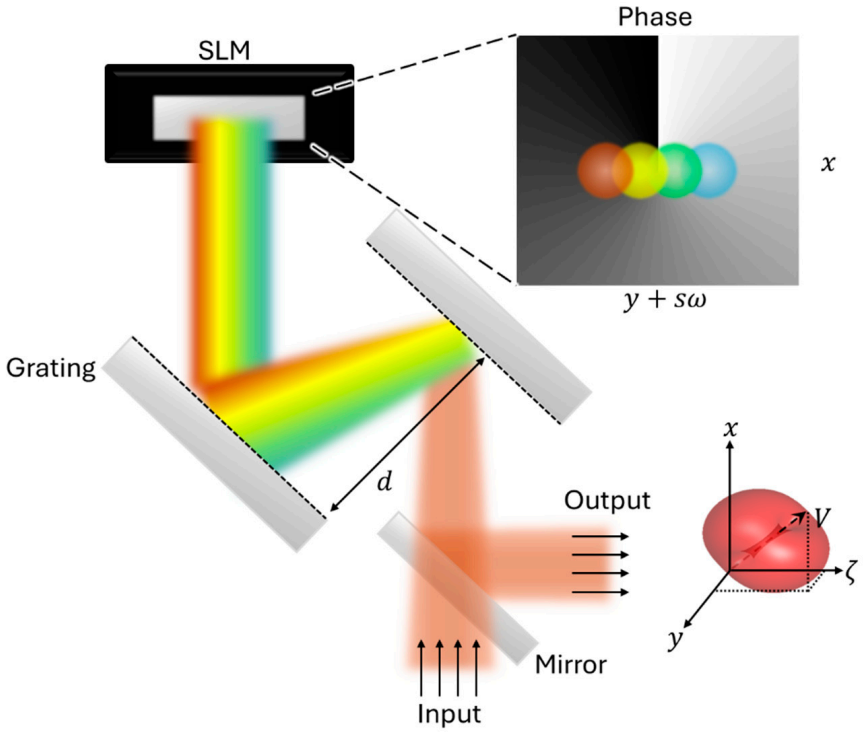

Figure 1. A grating pair enables high spatial chirp across the SLM plane without spatial focusing. This generates a tilted vortex outside the grating pair shaper.

The approximate spatial distance spread per frequency, which we define as the spatial chirp, is one factor that will be shown to directly control the initial tilt angle. As the spatial chirp increases, the tilt angle becomes more transverse to the propagation direction. We can approximate the spatial chirp as $s \approx \tan\left(\frac{d\theta}{d\lambda}\,\Delta\lambda\right)\frac{d}{\Delta\omega}$, where $\frac{d\theta}{d\lambda}$ is the grating's angular dispersion, d is the grating pair separation, and $\Delta\lambda$ and $\Delta\omega$ are the spectral bandwidth in wavelength and frequency. Two other factors that directly affect the tilt angle are the initial temporal dispersion of the pulse, D_o, and the dispersion acquired from traveling double passes through the grating pair, $D = -\frac{\lambda^3 d}{2\pi c^2 d_g^2 \cos(\theta_i)}$, where the grating pair has groove density d_g, separation d, and light incident angle θ_i [0]. One final factor that can alter the tilt angle is the initial beam size, w_{xy}^o, but this effect on tilt angle is not immediate, and is only seen after propagation.

With these factors in mind, we begin our analysis by finding the electric field immediately after receiving the phase modulation at the SLM plane located at $z = z_o$,

$$E(x, y, z_o, \omega) \propto (lx + i(y + s\omega))u_o(x, y, z_o, \omega) \quad (1)$$

where the initial complex envelope is $u_o = exp\left(-\frac{1}{w_{xy}^{o\,2}}(x^2+y^2) - \omega^2\left(\left(\frac{w_\zeta^o}{c}\right)^2 - i\pi(D+D_o)\right)\right)$. Additionally, l can equal +1 or −1, which controls the sign of the topological charge.

Now that we found the initial field in the temporal frequency domain, we can now find how the electric field changes with propagation in the time domain. First, we take the Fourier transform along the temporal frequency domain to find the field in the time domain. Secondly, we use angular spectrum Fresnel propagation to obtain the field at a distance of z. The angular spectrum method takes the Fourier space of the field at an initial location and adds a propagation phase to find the field at a second location: $E(x,y,z) = \mathcal{F}_{k_xk_y}\left\{\widetilde{E}(k_x,k_y,z_0)\exp\left(i\pi\lambda z\left(k_x^2+k_y^2\right)\right)\right\}$. Taking the temporal frequency Fourier transform along with the Fresnel propagation of Equation (1) gives

$$E(x,y,z,\zeta) \propto \left(lxM_{xy}(z) - s\zeta M_\zeta + iyM_{xy}(z)\right)u(x,y,z,\zeta) \tag{2}$$

where the envelope is $u = exp\left(-(x^2+y^2)\left(\frac{1}{w_{xy}(z)^2} - iC(z)\right) - \zeta^2\left(\frac{1}{w_\zeta(z)^2} - iC_\gamma\right)\right)$ and $\zeta = ct$. The complex coefficient on the x and y terms from propagation is $M_{xy} = \frac{w_{xy}^o}{w_{xy}}\exp(-i\psi_x)$, where the beam profile is $w_{xy} = w_{xy}^o\sqrt{1+\left(\frac{z}{z_r}\right)^2}$, the Gouy phase is $\psi = \text{atan}\left(\frac{z}{z_r}\right)$, and Rayleigh length is $z_r = \pi\left(w_{xy}^o\right)^2/\lambda$. The spatial and temporal quadratic phases are $C(z)$ and C_γ, which do not affect the vortex angle and therefore can be ignored. Finally, the complex coefficient on the ζ term is $M_\zeta = \frac{c}{w_{\zeta o}w_\zeta}\exp(-i\psi_\zeta)$ where the pulse width is $w_\zeta = w_{\zeta o}\sqrt{1+\left(\frac{c^2(D+D_o')}{\pi w_{\zeta o}^2}\right)^2}$ and the effective Gouy phase is $\psi_\zeta = \text{atan}\left(\frac{c^2(D+D_o)}{\pi w_{\zeta o}^2}\right)$.

The line where the real and imaginary parts of Equation (2) are simultaneously zero defines the orientation of the vortex. From Equation (2), a vector describing this orientation is calculated by finding the orientation of this line which gives [11]

$$V = \begin{pmatrix} -\left|M_{xy}\right|\left|M_\zeta\right|s\cos(\psi-\psi_\zeta) \\ l\left|M_{xy}\right|\left|M_\zeta\right|s\sin(\psi_\zeta-\psi) \\ l\left|M_{xy}\right|^2 \end{pmatrix} \tag{3}$$

which for propagation $z \gg z_r$ becomes

$$V \approx (z_r/z)^2\begin{pmatrix} -\frac{z}{z_r}\left|M_\zeta\right|s\cos(\psi_\zeta) \\ -\frac{z}{z_r}l\left|M_\zeta\right|s\sin(\psi_\zeta) \\ l \end{pmatrix} \tag{4}$$

It is now clear from Equation (4) that the vortex orientation is a function of the spatial chirp s, initial dispersion D_o, grating pair dispersion D, and initial beam size w_{xy}^o, and the sign of the topological charge l.

The vortex orientations are plotted in Figure 2a for different values of spatial chirp, with a new distance parameter $r = z/z_r$, and $l = 1$ for a femtosecond pulse of the typical experimental values with 40 nm bandwidth centered at $\lambda_o = 1$ µm. Since the Gouy phase and broadened beam size depend only on the ratio of the propagation distance to the Rayleigh length, the results are plotted as a function of r instead of z. For a fixed propagation distance, it is possible to adjust w_{xy}^o and s to control the vortex orientation. The vortex direction vector V can be represented as a point on a unit sphere. Two cases corresponding to two quadrants ($l = 1$ or $l = -1$) are shown in Figure 2, indicating that the sign of the topological charge flips the sign of the V_y and V_z. Examples of vortex

propagation are shown with iso-intensity plots in Figure 2c–e. From the perspective of the expanding wavepacket, the vortex angle does not appear to change with propagation within the wavepacket. However, Figure 2f–h plots the same examples from the perspective of a fixed volume, revealing that the vortex angle steadily changes with propagation.

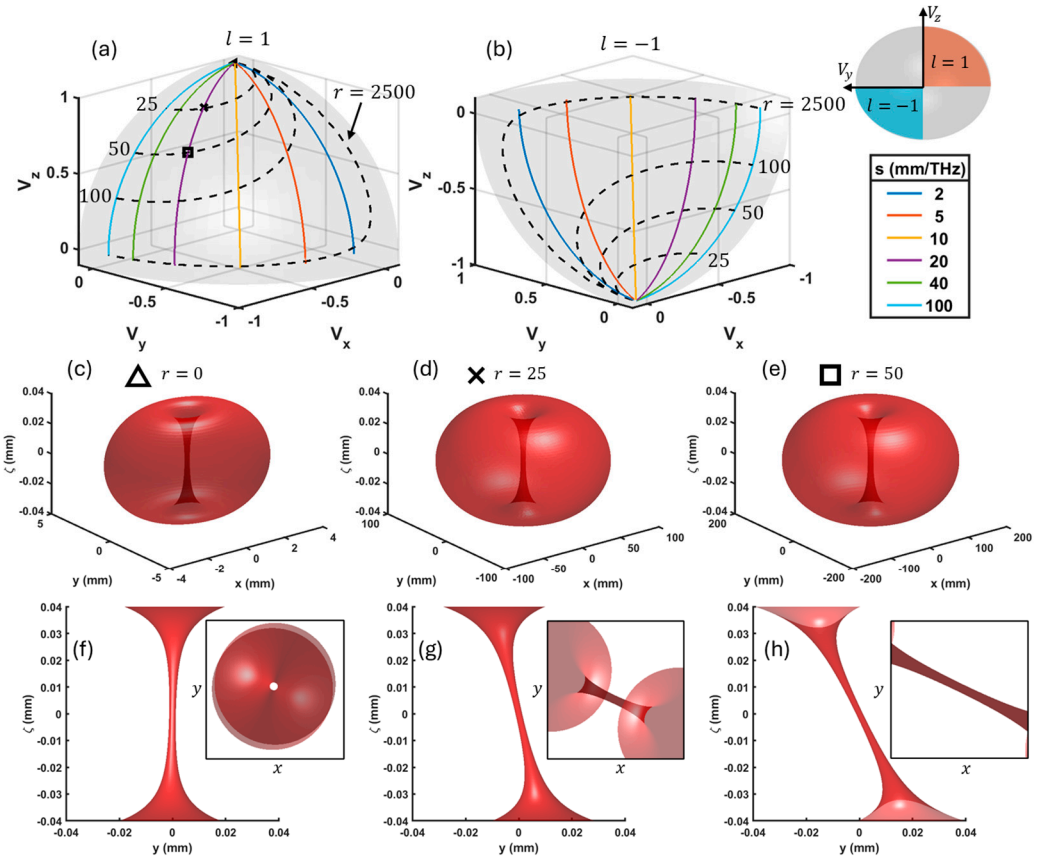

Figure 2. Vortex orientation of different spatial chirps plotted over variable $r = \frac{\lambda z}{\pi w_{xy}^2}$ values (**a**) for $l = 1$ and (**b**) $l = -1$, where the dashed lines are constant r values. The hemisphere with blue and red coloring on the top right shows the relative orientation of the positive and negative topological charges. Iso-intensity plots showing (**c**–**e**) entire wavepacket and (**f**–**h**) internal vortex in a fixed volume. The inset on (**f**–**h**) shows an alternative perspective.

The initial dispersion can also be adjusted independently of the spatial chirp. Figure 3 shows the vortex orientation for various spatial chirp values plotted against different D_o at $r = 1000$. The plot shows that the vortex direction rotates around the V_z axis as D_o changes. Constant D_o lines are also shown with dashed lines in the figure. By adjusting D_o and the spatial chirp s, it is possible to reach any point on two quadrants of the sphere, indicating any vortex orientation, at a fixed z location. Examples are also shown in Figure 3c,d with the iso-intensity plots of the vortex for different initial dispersion values, illustrating the strong effect on vortex orientation.

The aperture of the SLM can limit the maximum initial beam size and therefore restrict the beam to a high divergence angle which may be undesirable for long-distance applications. To overcome this, a telescopic beam expander system can be used to enhance the initially limited beam size at a long distance (Figure 4a,b). The system in Figure 4a is a combination of two positive lenses to increase the beam size while modifying the initial x and y component ratio in Equation (3): $\left|V_{x/y'}\right| \rightarrow -\left|\frac{f_2}{f_1}\right| |V_{x/y}|$. This setup changes the sign of the V_x and V_y components. The second system in Figure 4b uses one negative lens and one positive lens. This case also modifies the initial x and y in Equation (3) to

$\left|V_{x/y}{}'\right| \rightarrow \left|\frac{f_2}{f_1}\right|\left|V_{x/y}\right|$. For this second system, the sign of the V_x and V_y components are not altered.

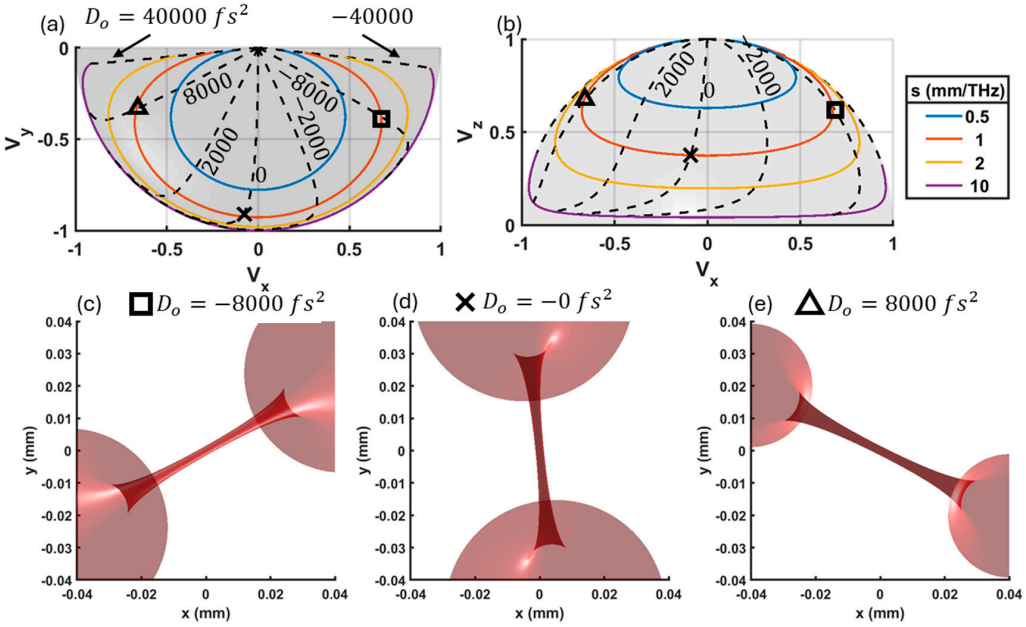

Figure 3. Vortex orientation at $r = 1000$ for different spatial chirps plotted over variable initial dispersions D_o with a (**a**) top view and (**b**) side view. (**c**–**e**) The iso-intensity plots of vortex inside wavepacket for different initial dispersion values at $s = 1$ mm/THz.

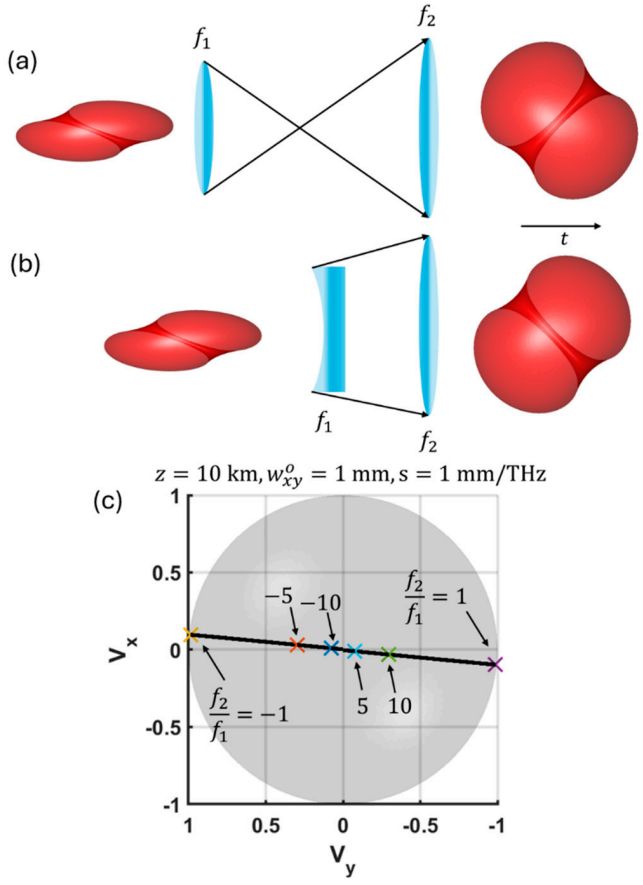

Figure 4. Telescope systems for increasing beam size and controlling vortex orientation. (**a**) Two positive focal length lenses that switch the signs of the V_x and V_y components. (**b**) A combination of negative and positive focal length lenses. (**c**) Vortex orientation at z = 10 km for various magnifications

f_2/f_1 with an input beam size of 1 mm and spatial chirp s = 1 mm/THz is given with the black line and a few magnifications are highlighted with markers.

The vortex orientation of a telescopic beam expander system with different magnifications at $z = 10$ km after the telescope is shown in Figure 4c. For this study, the initial beam size before magnification was set to 1 mm while the spatial chirp was chosen to be 1 mm/THz. While the 1 mm beam would have spread to ~1.6 m at this distance, a 20 mm beam formed with a $\frac{f_2}{f_1} = 20$ telescope would only expand to 160 mm due to the much narrower divergence angle. The plot also shows that increasing the magnification decreases the V_z component relative to V_x and V_y at a given distance. As the negative magnification switches the sign of the V_x and V_y components, the telescope systems in combination with controlling the sign of topological charge and initial dispersion means all the vortex orientation angles can be generated.

3. Discussion

The previous results reveal that tilted vortices can be generated at arbitrary angles at a desired location using a relatively simple laboratory setup. While not discussed, the spatial light modulator can easily apply higher topological charge phases. However, unlike optical vortices, higher topological charge spatiotemporal vortices and tilted vortices break up into separate vortices with propagation [5,6]. This break-up could be compensated for at a particular location by adjusting the phase pattern on the SLM. While any angle is possible to be generated, certain angles may be impractical to realize at a particular location for a given optical system. For example, it may be impractical to achieve $r = 1$ at $z = 10$ km, which would require a beam size of ~80 mm for $\lambda = 1$ μm. As SLMs are limited in size to <20 mm × 20 mm, a large telescope would be needed to achieve such a beam size. Additionally, for a given SLM size, the temporal frequency bandwidth of the pulse will determine how much spatial chirp can be obtained before the high- and low-frequency components are cropped by the SLM active area.

Given the limited theoretical concepts for tilted vortex generation [7–11] and only two experimental demonstrations [7,8], we believe this technique will be valuable for future tilted vortex applications. Compared to references [7,8], which achieved tilted vortices near a focus, the presented method can be used for longer-distance propagation. As another comparison, the work in reference [9] provides a theory for generating arbitrary tilted vortices by passing light through a specifically designed photonic crystal. The tilt angle can be tuned on-demand by rotating the crystal relative to the input beam. Such a device would be extremely valuable for generating tilted vortices given its compact nature. However, the custom device could be costly or difficult to make for some groups looking to use tilted vortices for applications. Additionally, the topological charge is fixed, while the presented method allows arbitrary topological charge. For these reasons, we believe the grating pair setup offers a convenient approach using common off-the-shelf components that can be easily adopted for future applications.

4. Conclusions

In conclusion, spatiotemporal vortices can be crafted with arbitrary tilt angles at a given distance. By controlling parameters such as the topological charge, spatial chirp, initial dispersion, beam size, and telescope setting, spatiotemporal vortices with any desired tilt angle can be crafted at a specific distance. The ability to achieve arbitrary vortex orientations at long propagation distances could offer significant advantages for long-distance communication applications.

Author Contributions: J.A. conducted the theoretical and numerical simulations. A.C. supervised the project. J.A. and A.C. wrote the manuscript. All authors have read and agreed to the published version of the manuscript.

Funding: This work is supported by a 2-year research grant from Pusan National University.

Data Availability Statement: The raw data supporting the conclusions of this article will be made available by the authors on request.

Conflicts of Interest: The authors declare no conflicts of interest.

References

1. Shen, Y.; Wang, X.; Xie, Z.; Min, C.; Fu, X.; Liu, Q.; Gong, M.; Yuan, X. Optical vortices 30 years on: OAM manipulation from topological charge to multiple singularities. *Light Sci. Appl.* **2019**, *8*, 90. [CrossRef] [PubMed]
2. Gao, D.; Ding, W.; Nieto-Vesperinas, M.; Ding, X.; Rahman, M.; Zhang, T.; Lim, C.; Qiu, C.W. Optical manipulation from the microscale to the nanoscale: Fundamentals, advances and prospects. *Light Sci. Appl.* **2017**, *6*, e17039. [CrossRef] [PubMed]
3. Płocinniczak, Ł.; Popiołek-Masajada, A.; Masajada, J.; Szatkowski, M. Analytical model of the optical vortex microscope. *Appl. Opt.* **2016**, *55*, B20–B27. [CrossRef] [PubMed]
4. Wang, J. Advances in communications using optical vortices. *Photonics Res.* **2016**, *4*, B14–B28. [CrossRef]
5. Hancock, S.W.; Zahedpour, S.; Goffin, A.; Milchberg, H.M. Free-space propagation of spatiotemporal optical vortices. *Optica* **2019**, *6*, 1547–1553. [CrossRef]
6. Chong, A.; Wan, C.; Chen, J.; Zhan, Q. Generation of spatiotemporal optical vortices with controllable transverse orbital angular momentum. *Nat. Photonics* **2020**, *14*, 350–354. [CrossRef]
7. Zang, Y.; Mirando, A.; Chong, A. Spatiotemporal optical vortices with arbitrary orbital angular momentum orientation by astigmatic mode converters. *Nanophotonics* **2022**, *11*, 745–752. [CrossRef] [PubMed]
8. Adams, J.; Chong, A. Tilted spatiotemporal optical vortex with partial temporal coherence. *Chin. Opt. Lett.* **2023**, *21*, 120002. [CrossRef]
9. Wang, H.; Guo, C.; Jin, W.; Song, A.Y.; Fan, S. Engineering arbitrarily oriented spatiotemporal optical vortices using transmission nodal lines. *Optica* **2021**, *8*, 966–971. [CrossRef]
10. Porras, M.A. Spatiotemporal optical vortex solitons: Dark solitons with transverse and tilted phase line singularities. *Phys. Rev. A* **2021**, *104*, L061502. [CrossRef]
11. Adams, J.M. Spatiotemporal Optical Vortex Phenomena. Doctoral Dissertation, University of Dayton, Dayton, OH, USA, 2024.